Averaging Semiempirical NMR Chemical Shifts: Dynamic Effects on the Subpicosecond Time Scale†

Tell Tuttle*

WestCHEM, Department of Pure and Applied Chemistry, University of Strathclyde, Thomas Graham Building, 295 Cathedral Street, Glasgow G1 1XL, United Kingdom

Received: March 30, 2009; Revised Manuscript Received: June 25, 2009

The variation of the ^{1}H and ^{13}C NMR chemical shifts of heptapeptide ATWLPPR was investigated during a hybrid quantum mechanical (QM)/molecular mechanical (MM = CHARMM) molecular dynamics simulation of the peptide in aqueous solvent. The semiempirical method OM3 was used as the QM method, and the effect of augmenting the OM3 Hamiltonian with an empirical dispersion term (OM3-D) was also explored. The semiempirical MNDO method was used to calculate the chemical shifts of snapshots taken at 50 fs intervals during the 100 ps simulation. The calculated chemical shifts are highly sensitive to fluctuations of the molecular geometry on the time scale of molecular vibrations. However, the time-averaged chemical shift over the full simulation results in reasonable agreement with the experimental NMR chemical shifts and more consistent results compared with the averaged chemical shifts obtained from gas-phase optimized conformations of the peptide. The OM3 and OM3-D methods are stable and reproduce the main features of the experimental geometry during the 100 ps simulation.

1. Introduction

Nuclear magnetic resonance (NMR) chemical shifts are widely recognized as one of the most important tools in biochemical structure determination because they encode structural information about the molecule itself and its surroundings.[1] A complete structural determination by NMR often requires a combination of various parameters; however, the chemical shifts are often critical in refining the biomolecular structure.[2−5] Moreover, there is a growing use of chemical shift data in the study of biomolecular interactions, such as ligand binding studies, where its use as a screening tool in the lead optimization process of drug discovery has become increasingly prevalent.[6]

NMR chemical shifts are sensitive to subtle changes in the electronic structure. These include changes in the molecular geometry, electrostatic interactions with the environment, the formation of inter- and intramolecular hydrogen bonds, and magnetic susceptibility effects. All of these effects are included in a quantum mechanical (QM) description of the system, and as such, at the QM level of theory, chemical shifts can be calculated with reasonable accuracy. Indeed, it has been demonstrated that ^{1}H and ^{13}C chemical shifts calculated using reasonable basis sets in conjunction with density functional theory (DFT) result in excellent agreement with experimental values for a variety of organic molecules.[7] Unfortunately the computational cost associated with using a reasonable basis set (typically of triple-ζ quality with additional diffuse and polarization functions) excludes their application to large systems (>100 atoms) or over long simulation time scales (>10 ps).

Given the desire of chemists to employ NMR techniques in the study of larger, biological systems, empirical (molecular mechanics (MM)) methods were developed to reproduce measured chemical shifts by parametrization and have proven to be useful in protein structure refinement.[8,9] However, these empirical approaches are limited in their application because they apply only to the residues included in the parametrization set (typically standard amino acids), and thus each new ligand or residue needs to be parametrized from scratch.

In the current work, the stability of the middle ground between the QM and MM approaches to calculating NMR chemical shifts is explored. The calculation of NMR chemical shifts using semiempirical methods has been an area of interest for some time[10] and has become more promising since the work of Patchkovskii and Thiel, where a set of parameters specifically for the calculation of H, C, N, and O chemical shifts was developed with excellent results relative to experimental values.[11] There have been a number of applications of this semiempirical method with consistently reliable results for optimized structure since its inception.[12−20] Recent work by Merz and coworkers[21] has resulted in the inclusion of ^{19}F parameters consistent with the previous parameter set,[11] and again with impressive results given the simplifications present in the semiempirical framework.

In previous studies at the QM and semiempirical levels of theory, the NMR chemical shifts have been calculated primarily on the basis of optimized structures. However, as the use of QM/MM methods are increasingly applied to study the dynamic behavior of compounds in solution via molecular dynamics (MD) simulations, it is important to assess the accuracy of the semiempirical method to predict the chemical shift values at nonequilibrium geometries. Experimentally, chemical shift measurements are time-averaged over a multitude of dynamic motions that occur on a subpicosecond-to-millisecond time scale. The effects of these motions on NMR chemical shifts can be categorized on the basis of the time scale on which they occur, namely, (a) the conformational changes that are observed on the millisecond time scale and (b) the bond vibrations that occur on the subpicosecond time scale. Previous work has investigated the possibility of utilizing calculated chemical shift data to differentiate between the conformational clusters that arise on the longer time scales.[22] However, the ability of the semiempirical method to determine the variation of ^{1}H and ^{13}C NMR

† Part of the "Walter Thiel Festschrift".

* Corresponding author. E-mail: tell.tuttle@strath.ac.uk.

10.1021/jp902875d CCC: $40.75
Published on Web 07/24/2009

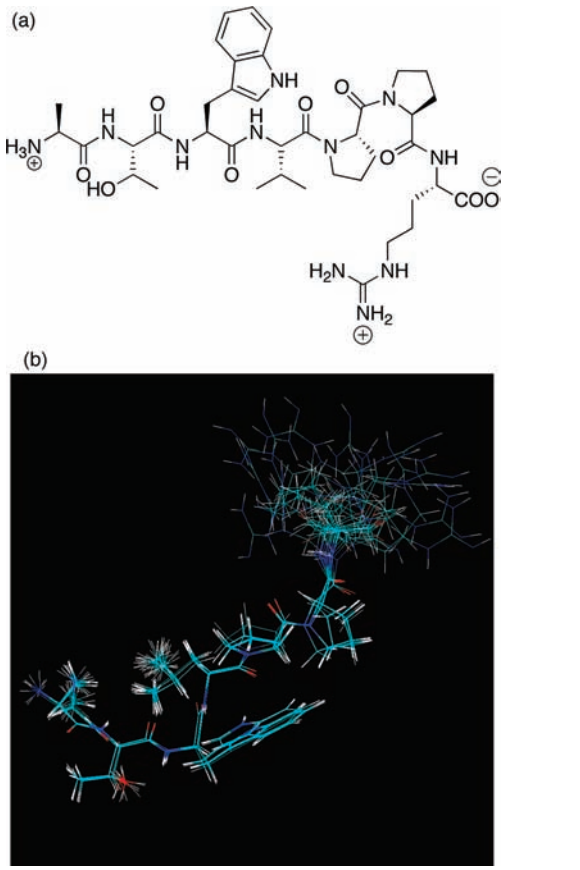

Figure 1. (a) Structure of heptatpeptide ATWLPPR (A7R). (b) Overlay of the 20 lowest-energy DYANA conformers (PDB ID: 2JP5).

chemical shifts accurately on the much shorter time scale of molecular vibrations has not yet been explored. For the data obtained from a QM/MM MD simulation to be useful in the determination of conformational effects on the chemical shifts, the method employed must inherently be stable on the shorter time scale to cope with the molecular vibrations that will also be observed during the simulation. Therefore, in the current study, the focus is on determining the stability of the method toward the dynamic effects (b) that occur on the subpicosecond time scale. The heptapeptide ATWLPPR is used for this case study.

Heptapeptide ATWLPPR (A7R, Figure 1) has been identified as a $VEGF_{165}$ selective inhibitor through binding to neuropilin-1 (NRP-1), where in vivo studies indicate that this inhibition results in decreased breast cancer angiogenesis and growth.[23] The peptide represents an important lead compound in the search for effective anticancer drugs, and as such, a detailed understanding of its structure and mode of interaction with NRP-1 is vital. NMR spectroscopy of the A7R structure in solution has recently been published and constitutes the reference data for the current study.[24]

The overlay of the 20 DYANA conformers of A7R, generated from the experimental NMR constraints (PDB ID: 2JP5),[24] shows a large degree of disorder in the terminal arginine residue (Figure 1b). If the terminal arginine residue is excluded, then the root-mean-square deviation (rmsd) of the twenty conformers from the average structure is only 0.42 Å. However, upon inclusion of the arginine residue, the rmsd, relative to the average structure, is increased to 1.22 Å. The terminal arginine group plays a key role in the binding of A7R to NRP-1, and an induced fit model of binding has been suggested on the basis of the disorder of the arginine group, which results from the empirical NMR fitting procedure.[24]

2. Computational Methods

The structure of the antiangiogenic heptapeptide ATWLPPR was obtained as twenty low-energy DYANA conformers using experimental NMR constraints (PDB ID: 2JP5).[24] The first conformer (model 1 in the PDB file) was chosen as the starting point for the QM/MM MD simulation. The peptide is simulated in an aqueous environment; therefore, the protonation states were assigned accordingly (i.e., the guanidinium group of arginine was protonated, the N-terminal (Ala-1) was assigned as CNH_3^+, and the C-terminal (Arg-7) was assigned as COO^-), resulting in an overall charge of +1 for the heptatpeptide.

The system was hydrated using the droplet model with a 25 Å sphere of equilibrated TIP3P water centered at the C^α atom of Pro-5. All waters that overlapped[25] with the peptide were deleted. The remaining water molecules were relaxed and subsequently subjected to a molecular dynamics run for 10 ps at 300 K using Langevin dynamics. A stochastic boundary potential[26] was used to maintain the structure of the water sphere, whereas the peptide was frozen during both the solvent geometry minimization and the solvent equilibration period. This hydration procedure was performed three times. All structure preparation calculations were carried out with the CHARMM program[27−29] using the standard CHARMM force field for proteins.[30]

The QM/MM calculations employed the OM3 semiempirical method[31] as the QM method, either in its standard form or with the empirical dispersion function (OM3-D) included.[32] In each case, the CHARMM force field was used for the MM part. The modular program package ChemShell[33,34] was used for all QM/MM calculations, where the QM energy and gradients were provided by a development version of MNDO04.[35] ChemShell's internal force field driver using the CHARMM parameter and topology data provided the MM energy and gradients. Electrostatic cutoffs were not employed in the QM/MM model, neither between the QM and MM regions nor within the MM region alone. The QM density was electrostatically embedded into the MM environment by including the point charges from the MM atoms into the QM Hamiltonian. The van der Waals interactions between the QM and MM regions were handled at the MM level, as previously described.[34] The QM region was defined as the full heptapeptide (122 atoms), and thus there are no covalent bonds forming a QM (peptide)−MM (solvent) boundary.

In the QM/MM MD simulation, an active subset of the total system is allowed to move, whereas the remaining atoms are frozen. The active subset was defined from the initial complex geometry using a distance criterion, whereby any residue that contains an atom within 16 Å of the C^α atom of Pro-5 is included. The resulting active region contains 2063 atoms, about one-third of the total system size 6512 atoms.

The MD simulations were performed under NVT conditions at $T = 300$ K. During the heating phase (10 ps), the temperature was controlled by a Berendsen thermostat[36] with a coupling time of 0.1 ps. During the equilibration phase (100 ps), the Nosé−Hoover chain thermostat,[37−39] as implemented in the ChemShell dynamics module,[34] was used. All peptide hydrogen atoms were assigned the mass of deuterium, whereas the water molecules were kept rigid using SHAKE constraints.[40] The time step for both heating and equilibration was 1 fs.

QM geometry optimizations were performed with HDLCOpt,[41] a linear scaling, microiterative algorithm that employs a set of hybrid delocalized coordinates, as implemented in ChemShell. The residues defined for HDLCOpt were taken as

the standard CHARMM residues. The optimization of the 20 DYANA conformers in the gas phase was carried out at the OM3 and OM3-D levels of theory. The protonation state of arginine and the terminal residues were assigned to each conformer, as described above.

The calculation of the chemical shifts at the semiempirical level of theory was carried out in the framework of the MNDO Hamiltonian[42] using gauge-including atomic orbitals (GIAO).[43,44] The "method B" parameters developed for the calculation of NMR chemical shifts for H, C, N, and O were employed.[11] To investigate the variation of the chemical shifts over the simulation period, snapshots of the MD simulation were obtained every 50 fs, after equilibration, resulting in 2000 snapshots for each simulation. The structures obtained from the simulation underwent no further structural refinement; that is, the NMR calculations were performed as single-point calculations on the snapshot structures. This is consistent with the goal of the study, that is, to capture the effect of the molecular vibrations on the chemical shift, as the gas-phase optimization/refinement of the structures would simply result in equilibrium values.

The NMR calculation of each snapshot was performed in the absence of the water environment because the semiempirical NMR chemical shifts ($\delta = \sigma_{ref} - \sigma$) have been scaled to reproduce the experimental chemical shifts in water from the gas-phase calculation of the absolute isotropic shielding (σ) through the optimization of the σ_{ref} value for this environment.[11] To include the electrostatic effects of the environment into the Hamiltonian via a QM/MM approach, one should additionally reparameterize the NMR shift parameters to account for this perturbation in the optimization function.

The optimization of conformer 1, using DFT, was also carried out with the HDLCOpt optimization algorithm[41] implemented in ChemShell, where the energy and gradients were provided by TurboMole.[45−48] The DFT optimizations were performed at the RI[49]-BP86[50−52]/def2-SVP[53] level of theory. The BP86 functional was augmented with the Grimme empirical dispersion term (BP86-D),[54] as implemented in ChemShell. The isotropic shieldings were calculated using the GIAO method, as implemented in Gaussian 03.[55] The calculations were performed at the B3LYP[50,52,56−59]/6-311++G(d,p)[60,61] level of theory, which has previously been shown to provide reliable results for NMR chemical shifts.[62] NMR calculations at the DFT level of theory were carried out on the RI-BP86-D/def2-SVP-optimized geometries. The isotropic shieldings were converted to chemical shifts using the calculated average ^{1}H and ^{13}C NMR shieldings of tetramethylsilane (TMS) as the reference values.

3. Results and Discussion

A. Semiempirical Nuclear Magnetic Resonance Chemical Shift Calculations on Optimized Structures. The comparison of the calculated NMR shifts during the MD simulation assumes that the computational method employed is able to represent the geometric and electronic features of the system adequately. Therefore, an initial test of the OM3 and OM3-D methods for reproducing the peptide structure in the gas phase was carried out, and for each optimized conformation, the ^{1}H and ^{13}C NMR chemical shifts were calculated. In addition, the lowest-energy DYANA conformer (Conf-1) was also optimized at the RI-BP86-D level of theory to calculate the chemical shifts at the DFT level of theory. (See the Computational Methods.) The coordinates for all optimized geometries are available in the Supporting Information (XYZ format).

The root-mean-square deviation (rmsd) of the backbone atoms from the optimized structures does not deviate significantly from the starting (DYANA) geometries obtained from the PDB file. The OM3-D-optimized structures are, on average, slightly better than those obtained from the OM3 optimization with an average rmsd for the 20 conformers of 1.20 and 1.45 Å, respectively (Table 1). Moreover, the structures obtained from OM3-D are more consistently closer to the DYANA geometry with a maximum backbone rmsd of 1.64 Å for Conf-8, whereas the maximum backbone rmsd for the OM3-optimized structures is 2.48 Å (Conf-20). The inclusion of all heavy (non-H) atoms into the alignment of the structures and the rmsd calculation results in a clearer distinction between the OM3 and OM3-D methods. The average rmsd for the OM3-D optimized structures is increased slightly to 1.43 Å as a result of including the amino acid side chains into the alignment. However, the average rmsd of the OM3-optimized structures is increased to 2.25 Å, with a maximum heavy atom rmsd of 3.56 Å occurring for Conf-20 (Table 1). The inclusion of the dispersion function in the OM3-D method provides a more realistic description of the aromatic tryptophan (Trp-3) side chain. In the OM3 description, there are no stabilizing interactions between this side chain and the remainder of the peptide, and as such, the side chain rotates to allow more stabilizing interactions elsewhere in the peptide. In the gas-phase OM3-D description, the Trp-3 side chain will experience some weak dispersion interactions with the proximal backbone H atoms of A7R that stabilize its orientation.

TABLE 1: RMSD of the OM3- and OM3-D-Optimized Conformers Relative to the DYANA Structures[a]

conformer	OM3(back)	OM3-D(back)	OM3(heavy)	OM3-D(heavy)
Conf-1	1.14	1.11	2.36	1.21
Conf-2	1.36	1.34	2.91	1.64
Conf-3	1.22	1.14	2.36	1.56
Conf-4	1.41	1.11	3.04	1.46
Conf-5	1.26	1.16	2.09	1.92
Conf-6	1.77	1.60	2.15	1.82
Conf-7	1.90	1.40	3.19	1.48
Conf-8	1.64	1.64	1.59	1.59
Conf-9	1.50	1.54	2.05	2.21
Conf-10	1.71	1.09	2.96	1.40
Conf-11	1.02	0.85	2.07	1.00
Conf-12	1.28	0.82	2.05	1.14
Conf-13	1.15	1.07	1.55	1.31
Conf-14	1.31	1.29	1.35	1.27
Conf-15	1.64	0.98	2.71	1.06
Conf-16	1.46	1.31	2.01	1.47
Conf-17	1.37	1.35	1.39	1.33
Conf-18	1.34	1.10	2.23	1.26
Conf-19	1.01	0.99	1.46	1.11
Conf-20	2.48	1.01	3.56	1.38
average[b]	1.45	1.20	2.25	1.43

[a] All values are in angstroms. OM3(back) and OM3-D(back) designate the rmsd of the backbone atoms for the OM3- and OM3-D-optimized structures, respectively, which have been aligned with the backbone atoms of the DYANA conformer. OM3(heavy) and OM3-D(heavy) designate the rmsd of all non-H atoms after the OM3 and OM3-D structures, respectively, which have been aligned with all non-H atoms of the DYANA conformer. [b] Average is the mean rmsd for all 20 conformers at a given optimization and alignment.

The BP86-D-optimized structure of Conf-1 is similar to that obtained from the OM3-D optimization (compare blue and green structures in Figure 2). The backbone rmsd for the BP86-D-optimized structure is 1.54 Å, relative to the DYANA Conf-1 geometry, whereas the heavy atom rmsd is increased slightly to 1.78 Å at the DFT level. The primary difference between the BP86-D structure and the OM3-D structure is a rotation of the N-terminal Ala-1 residue. In the BP86-D optimized structure,

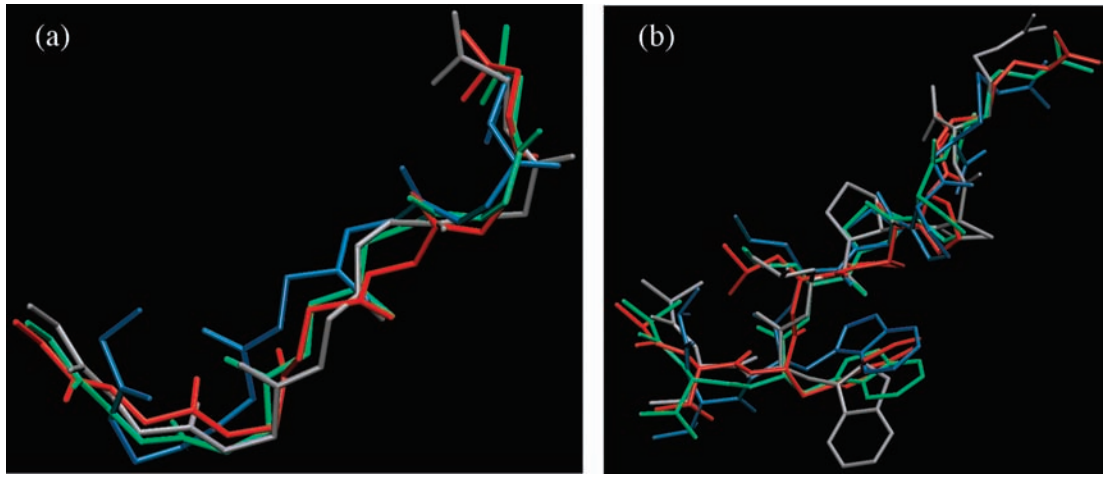

Figure 2. Overlay of OM3-, OM3-D-, and BP86-D-optimized structures of Conf-1, with the DYANA structure. (a) Alignment of backbone atoms. (b) Alignment of all non-H atoms. Color code: DYANA structure, red; OM3-optimized structure, silver; OM3-D-optimized structure, green; BP86-D-optimized structure, blue.

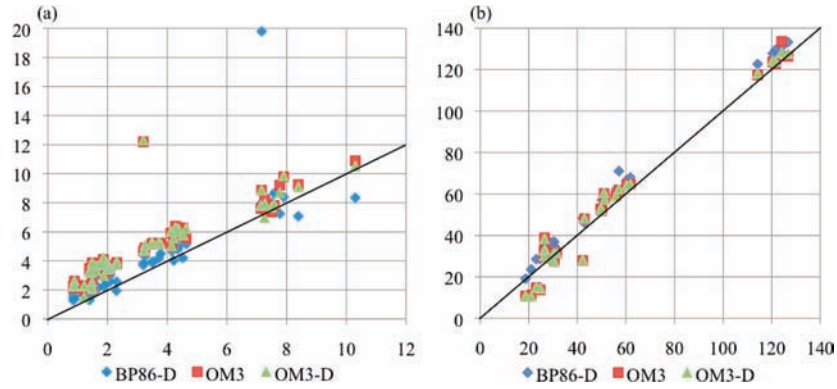

Figure 3. DFT and semiempirical chemical shifts of the optimized Conf-1 structures as a function of the experimental chemical shifts. (a) ^{1}H NMR chemical shifts. (b) ^{13}C NMR chemical shifts. BP86-D refers to the DFT chemical shifts calculated at the BP86-D optimized geometry. OM3 and OM3-D refer to the semiempirical chemical shifts calculated at the OM3 and OM3-D optimized geometries, respectively. Experimental values correspond to the abscissa, with calculated values along the ordinate; all chemical shifts are in ppm.

the positively charged N-terminus rotates to form a strong ionic bond (1.53 Å) with the backbone carbonyl group of the Trp-3 residue. In the OM3- and OM3-D-optimized structures, this H bond is not present, rather the NH_3^+ group forms a H bond with the carbonyl group of its own residue (Ala-1). It has previously been pointed out that the OMx methods generally underestimate H-bond lengths, particularly in the case of ionic H-bonds, as occurs in this case.[63] Strong ionic H bonds are also seen in all three of the optimized structures at the C terminus between the carboxylate group and the H atoms on the Arg-7 side chain. These strong ionic interactions are expected because the charged species are not well-stabilized in the gas phase. However, these unrealistically short H bonds are unlikely to play a role in the MD simulation, where the peptide is well-solvated. (See below.)

The experimental ^{1}H and ^{13}C NMR chemical shifts are not available for all H and C atoms in the heptapeptide. Therefore, whereas the chemical shifts for all H and C atoms were calculated, the discussion of the calculated chemical shifts concentrates only on those values that are available experimentally. The chemical shifts depend sensitively on the changes in the electronic structure of the compound, which are also reflected in variations in bond lengths and other internal coordinates. The semiempirical NMR method was parametrized on the basis of optimized B3LYP/6-311G** geometries, although the method also performs well for structures optimized at the constrained MNDO, AM1, and PM3 levels of theory.[11] Therefore, the transferability of these parameters to the OM3- and OM3-D-optimized structures was only assessed for the Conf-1 structure. The RI-BP86-D-optimized structure was used for the DFT NMR calculation, which was carried out at the B3LYP/6-311++G(d,p) level of theory.

The proton chemical shifts are predicted with reasonable accuracy in all but one case for each of the optimized structures (Figure 3a). For each optimized structure, the hydrogen involved in the strong ionic H bond with the carboxylate group of the Arg-7 (C-terminus) is strongly shifted relative to the experimental value. For the OM3- and OM3-D-optimized structures, this corresponds to the H^{δ} atom of the Arg-7 side chain, whereas in the BP86-D-optimized structure, the ionic H bond is formed with the H^{ε} of the Arg-7 side chain. These interactions are unlikely to exist in the fully solvated system. The mean unsigned error (MUE) of the ^{1}H NMR chemical shifts for Conf-1 is 0.94 ppm at the DFT level of theory. However, the standard deviation in the unsigned errors (σ_{UE}) for the ^{1}H NMR chemical shifts is 1.70 ppm because of the large error resulting from the ionic H bond in this structure. If the chemical shift of the H^{δ} atom is excluded from the analysis, then the MUE decreases to 0.71 ppm and σ_{UE} decreases to 0.46 ppm at the DFT level.

At the semiempirical level of theory, both the OM3- and OM3-D-optimized geometries result in an MUE of 1.52 ppm for the ^{1}H chemical shifts. However, as in the case of the DFT-optimized structure, the ionic H bond formed in the gas-phase optimization is an outlier that strongly distorts the results (OM3:

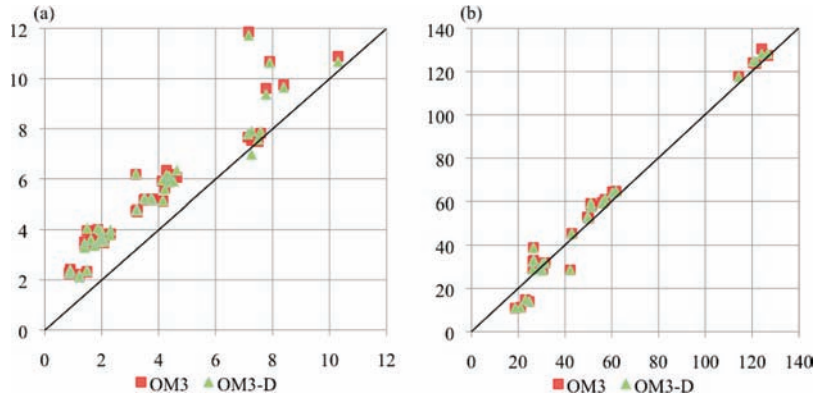

Figure 4. Averaged semiempirical chemical shifts for the 20 optimized conformers of A7R, as a function of the experimental chemical shifts. (a) ^{1}H NMR chemical shifts. (b) ^{13}C NMR chemical shifts. OM3 and OM3-D refer to the average semiempirical chemical shifts calculated from the OM3- and OM3-D-optimized geometries, respectively. Experimental values correspond to the abscissa, with calculated values along the ordinate; all chemical shifts are in ppm.

σ_{UE} = 1.17 ppm; OM3-D: σ_{UE} = 1.20 ppm). The exclusion of the outlier results in a decreased MUE of 1.38 ppm for both the OM3 and OM3-D optimized structures (OM3: σ_{UE} = 0.53 ppm; OM3-D: σ_{UE} = 0.56 ppm). The semiempirical NMR method appears to systematically overestimate the calculated chemical shielding for the OM3- and OM3-D-optimized structures. However, given the uncertainty in ascribing the experimental values to any individual conformer of A7R and the differences in the geometries of the experimental and optimized structures (Figure 2), an MUE of 1.38 ppm is acceptable.

The ^{13}C NMR chemical shifts for the optimized structures of Conf-1 also reproduce the experimental values with reasonable success (Figure 3b). The MUE for the DFT-calculated shifts of the BP86-D-optimized geometry is 6.30 ppm (σ_{UE} = 2.65 ppm), where the calculated values are generally larger than the experimental results. The MUE for the semiempirical chemical shifts are similar for the OM3- and OM3-D-optimized geometries (5.26 and 5.27 ppm, respectively) and slightly lower than the DFT results, although the distribution of the errors is larger for the semiempirical methods (OM3: σ_{UE} = 3.86 ppm; OM3-D: σ_{UE} = 3.60 ppm). Therefore, for both the ^{1}H and ^{13}C NMR chemical shifts, the semiempirical method performs as well as the DFT method, with both approaches slightly overestimating the chemical shifts for the optimized structures. Despite both the optimization method and NMR method differing, the calculated chemical shifts map closely, in all three models, onto those obtained experimentally. The individual chemical shifts calculated at the optimized Conf-1 geometries are available in Table S1 of the Supporting Information.

The 20 DYANA conformers were optimized at the OM3 and OM3-D levels of theory and the chemical shifts of each resulting conformation were determined using the semiempirical NMR method.[11] The average chemical shifts (δ_{AV}) were determined from the 20 optimized geometries for each atom where an experimental chemical shift was available. The OM3- and OM3-D-optimized geometries result in similar averaged chemical shift values (Figure 4; for a detailed comparison, see Table S2 in the Supporting Information) and identical trends; therefore, in the following, only the OM3-D results are discussed.

The MUE for the averaged ^{1}H chemical shifts (Figure 4a) is 1.52 ppm (OM3-D), which is similar to the result obtained for Conf-1 with all H atoms included. However, the averaged ^{13}C NMR results (Figure 4b) are slightly more favorable (MUE(OM3-D) = 5.04 ppm) than those obtained from the single Conf-1 structure. The lack of improvement in the ^{1}H NMR results is again due to the presence of the ionic H bond. However, the H atom involved in forming the ionic H bond varies between the different optimized conformers. In each case, this H atom experiences an unrealistic environment, relative to the experimental situation, and as such, there is a strong deviation between the calculated and experimental shift for the atom. Because the carboxylate is able to form a strong ionic interaction with different H atoms, depending on the starting conformation for the optimization, the ^{1}H chemical shifts for the H atoms proximal to the carboxylate of Arg-7 are negatively affected by the averaging procedure. Therefore, whereas the error is not localized to a single H atom, as in the case of Conf-1, the MUE is comparable, whereas the σ_{UE} is decreased to 0.72 ppm.

The variation in the ^{1}H chemical shifts value of a given atom for the different conformers is evidenced in the standard deviation of the chemical shifts for that atom (σ_{δ}). The largest ^{1}H σ_{δ}, for the OM3-D-optimized geometries, is 3.03 ppm (49% of the δ_{AV}), which occurs for the H$^{\varepsilon}$ atom of Arg-7 (δ_{AV} = 6.20 ppm). In contrast, the ^{13}C chemical shifts have relatively small standard deviations across the 20 optimized geometries, where the maximum σ_{δ} is 2.47 ppm (4% of the δ_{AV}), which occurs for the C$^{\alpha}$ atom of Arg-7 (δ_{AV} = 59.5 ppm). Given the large variation in the proton chemical shifts and the tendency of the structures to form ionic H bonds when optimized in the gas phase, it is clear that these gas-phase optimized structures are not reliable models for representing the solution phase structure from which the experimental values have been determined. In the following section, the effect of explicitly including solvent on the structure of the peptide is considered.

B. Time Evolution of Semiempirical Nuclear Magnetic Resonance Chemical Shifts. ***i. Structure.*** The lowest-energy model of the DYANA structures (Conf-1) was used as the starting structure for the MD simulation of the peptide in solvent. A7R was fully solvated in a sphere of TIP3P water molecules, and the system was allowed to equilibrate for 10 ps. Following this initial equilibration period, the MD simulation was carried out for a further 100 ps production run, as described in the Computational Methods section. Irrespective of the QM method applied in the simulation, the structure of the heptapeptide is clearly flexible; the rmsd (relative to the NMR structure) during the simulation is 2.609 Å at the OM3/CHARMM level of theory and 2.330 Å at the OM3-D/CHARMM level of theory (Table 2). In both the OM3 and OM3-D QM/MM MD simulations, the structure retains is extended conformation. The main noticeable deviation in the equilibrated structure, relative to the NMR structures, is the rotation of the Trp-3 side chain. At the OM3-D level, the Trp-3 residue has an rmsd of 3.224 Å (Table

TABLE 2: RMSD of the Full Peptide (A7R) and Its Constituent Residues, Excluding H Atoms[a]

	rmsd(OM3)	σ(OM3)	rmsd(OM3-D)	σ(OM3-D)
A7R	2.609	0.616	2.330	0.457
Ala-1	2.003	0.647	1.537	0.556
Thr-2	1.871	0.594	1.420	0.547
Trp-3	2.887	0.505	3.224	1.042
Leu-4	3.052	0.646	1.972	0.536
Pro-5	1.947	0.745	1.541	0.499
Pro-6	3.317	1.578	1.679	0.584
Arg-7	2.171	0.461	2.413	0.586

[a] rmsd is the average of the rmsd values, relative to the NMR structure, for the 2000 snapshots of the 100 ps production simulation. σ is the standard deviation of the rmsd values during the simulations. (OM3) refers to the QM/MM MD simulation, where QM = OM3; (OM3-D) refers to the QM/MM MD simulation, where QM = OM3-D. In both simulations, MM = CHARMM.

2), this corresponds to a rotation of the side chain from a closed position into a more solvent-exposed orientation. The driving force for this rotation is the ability of the side chain to form T-stacking interactions with water molecules on both sides of the aromatic ring, which are limited to one face in the closed structure.

The OM3-D method includes the accurate modeling of dispersion interactions between QM and QM atoms.[32] Therefore, if the closed conformation had dominant dispersion interactions between peptide atoms, then the mobility of the Trp-3 side chain aromatic ring would be decreased within the OM3-D/CHARMM description. However, the rmsd value for the Trp-3 actually increases for the OM3-D/CHARMM QM/MM method, relative to the OM3/CHARMM results, indicating that when solvated, the intramolecular dispersion interactions are not competitive with those formed between the Trp-3 ring and the water molecules. Visual inspection of the system confirms that the stacking interactions between the proximal proline residues and the Trp-3 side chain are less numerous than those obtained with solvent molecules because of steric constraints imposed by the peptide backbone.

At the OM3/CHARMM level, the Pro-6 residue, adjacent to the terminal arginine residue, also displays a high degree of flexibility. There is a concerted rotation about the backbone for the two residues (Leu-4 and Pro-6) adjacent to the central proline (Pro-5). This is reflected in the larger rmsd values for these residues at the OM3/CHARMM level, whereas no such rotation is observed at the OM3-D/CHARMM level of theory. In both simulations, the terminal arginine residue (Arg-7) is reasonably mobile (rmsd = 2.171 Å, OM3; rmsd = 2.413 Å, OM3-D; Table 2). However, because the positively charged guanidinium group is well-solvated in the extended structure, the mobility of the residue does not correspond to the formation of intramolecular ionic H bonds, as observed in the gas-phase optimized structures.

ii. Time-Averaged Nuclear Magnetic Resonance Chemical Shifts. The experimental NMR time scale is typically on the order of 10^{-3} s (ms), which is several orders of magnitude longer than the time scale investigated during the MD simulation, 10^{-10} s (100 ps). However, before one is able to address the conformational changes that occur on the ms time scale, the method employed must be stable toward molecular vibrations that occur on the subpicosecond time scale. Nonetheless, to compare the calculated chemical shifts with the experimental data, the average chemical shift from all snapshots is employed with the understanding that this does not represent a complete ensemble over the possible conformers of the peptide.

The time scale for individual bond vibrational motions is on the 10^{-15} s (fs) time scale, which is accessible in the current simulation that employs a 1 fs time step. The vibration of bonds involving H atoms is indeed faster than the 1 fs time scale would accurately model; however, rather than using a rigid constraint on the bonds involving H atoms, the mass of deuterium was substituted, which provides both flexibility to the X−H bonds and the possibility of using the larger (1 fs) time step. The snapshots, taken every 50 fs, provide a window into the effect of molecular vibrations on the magnitude of the NMR chemical shifts.

The time-averaged chemical shifts (δ_{TAV}) from Figure 5 are calculated as the average value of the chemical shift for each atom from the 2000 snapshots taken during the 100 ps MD simulation, that is, after the 10 ps equilibration period. The results of the OM3/CHARMM and OM3-D/CHARMM simulations are similar. (See Table S3 in the Supporting Information for a detailed comparison.) Therefore, in the following, only the results of the OM3-D/CHARMM simulation are discussed. The MUE of the ^{1}H δ_{TAV} values is slightly decreased, relative to the MUE obtained for the optimized conformers (MUE(δ_{AV})), to 1.44 ppm from the OM3-D/CHARMM simulation (Figure 5a), and the distribution of the unsigned errors (σ_{UE} = 0.57 ppm) is also improved. As was observed for the gas-phase optimized systems (Figure 4a), the semiempirical NMR method tends to overestimate the value of most of the ^{1}H NMR chemical shifts. Moreover, this overestimation is more consistent in the δ_{TAV} results (Figure 5a) relative to δ_{AV} (Figure 4a), an

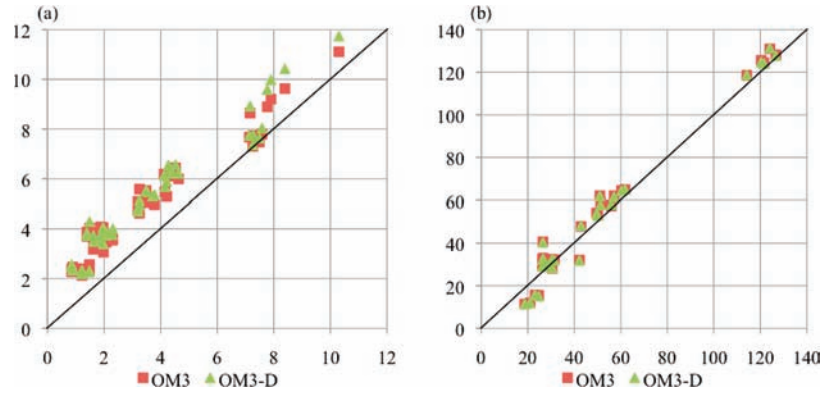

Figure 5. Time-averaged NMR chemical shifts from the MD simulation of A7R. (a) ^{1}H NMR chemical shifts. (b) ^{13}C NMR chemical shifts. OM3 and OM3-D refer to the averaged semiempirical chemical shifts calculated from the OM3/CHARMM and OM3-D/CHARMM MD simulation snapshots, respectively. Experimental values correspond to the abscissa, with calculated values along the ordinate; all chemical shifts are in ppm.

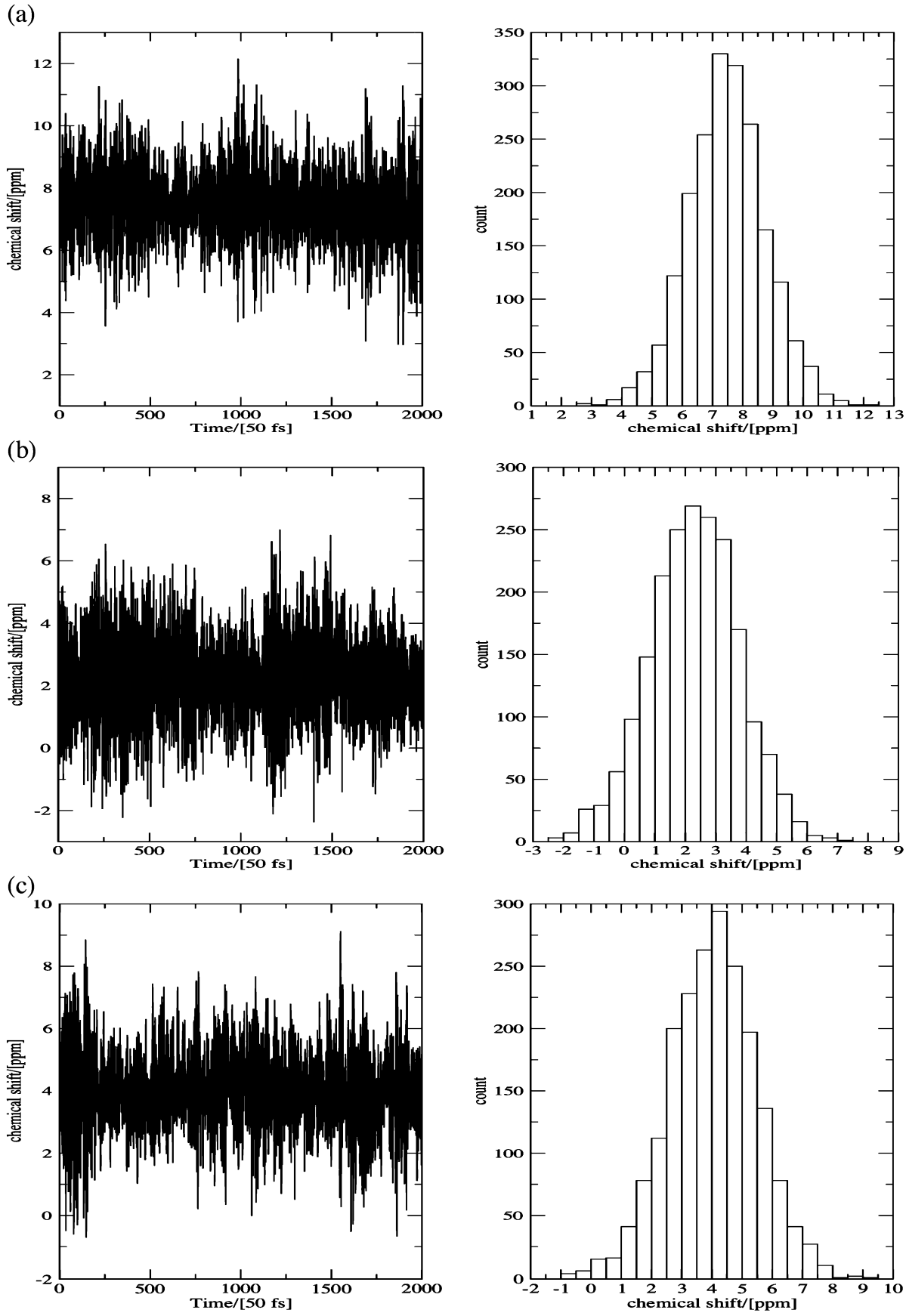

Figure 6. Time evolution of NMR chemical shifts for (a) H46: UE = 0.01 ppm; (b) H63: UE = 1.44 ppm; and (c) H59: UE = 2.55 ppm. Left: Variation in the ^{1}H NMR chemical shift as a function of time over the 100 ps simulation. Right: Distribution (bin width = 0.5 ppm) of the calculated chemical shifts for the 2000 snapshots taken at 50 fs intervals during the simulation.

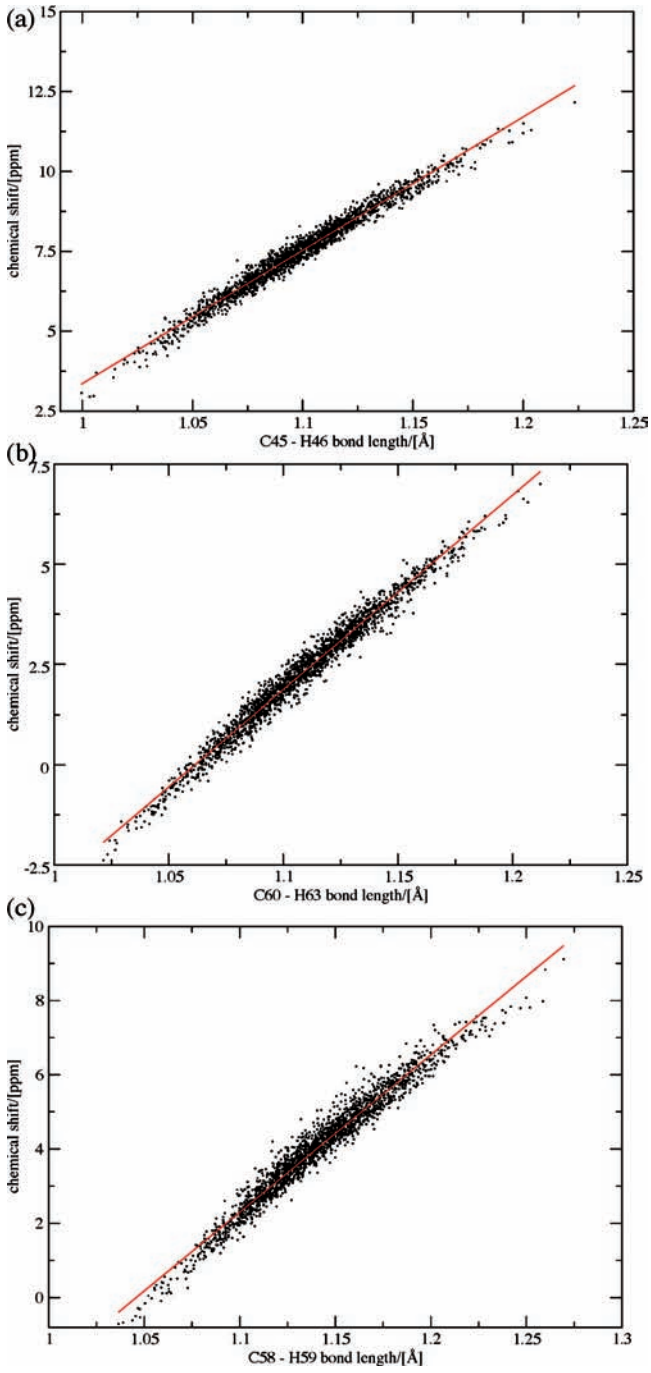

Figure 7. Correlation between the calculated chemical shift and the C−H bond length for (a) H46, (b) H63, and (c) H59.

observation that is quantitatively expressed in the lower σ_{UE} value. The exception to this systematic overestimation is the cluster of results around 7.0−7.5 ppm, which corresponds to the H atoms on the aromatic Trp-3 side chain. The semiempirical method performs remarkably well for the aromatic subset of atoms, with an MUE of 0.35 ppm.

The time-averaged ^{13}C chemical shifts again reproduce the experimental values reasonably well (Figure 5b). The MUE of the ^{13}C δ_{TAV} is 5.24 ppm, which is slightly larger than the MUE obtained for the optimized conformers (δ_{AV} = 5.04 ppm). However, the distribution of the errors is marginally improved (σ_{UE} = 3.38 ppm) as a result of the simulation in the aqueous environment.

The similarity in the calculated average chemical shifts from the 20 DYANA conformers and the time-averaged chemical shifts, δ_{AV} and δ_{TAV}, respectively, is surprising. This result suggests that either the conformational sampling in the 100 ps simulation is sufficient to cover the various conformers obtained from the DYANA analysis or that the semiempirical method is insensitive to the changes in the molecular geometry that occur on these time scales. To address this question, the following section investigates the time dependence of individual ^{1}H and ^{13}C chemical shifts for the atoms that have the smallest, mean, and largest unsigned errors from their respective sets.

iii. Time-Dependence of Nuclear Magnetic Resonance Chemical Shifts. The time dependence of the chemical shifts considers how the local fluctuations that occur for the molecular geometry on a femtosecond time scale (e.g., bond stretching, angle bending, etc.) as well as larger conformational changes in the structure (e.g., bond rotations, although in the current simulation, these are largely unsampled) influence the overall measured NMR chemical shift. To determine whether there is a relationship between these changes on the femtosecond time scale and the unsigned error in the resulting average value, the time evolution of representative cases is discussed below for both the ^{1}H and ^{13}C NMR results from the simulation of A7R. The representative H and C atoms were chosen to cover the ranges in the unsigned errors for the ^{1}H and ^{13}C time-averaged chemical shifts: H46 (H^{ζ} of the Trp-3 side chain, UE = 0.01 ppm); H63 (H^{δ} of the Leu-4 side chain, UE = 1.44 ppm); and H59 (H^{γ} of Leu-4 side chain, UE = 2.55 ppm) for the H atoms and C90 (C^{β} of the Pro-6 side chain, UE = 0.48 ppm); C108 (C^{δ} of the Arg-7 side chain, UE = 5.28 ppm); and C58 (C^{γ} of the Leu-4 side chain, UE = 13.89 ppm) for the C atoms.

Inspection of the left panels of Figure 6 reveals that there is a high degree of variability in the chemical shift during the MD simulation. For a given proton, the chemical shift varies by as much as 10 ppm between different snapshots. The linear relationship between the chemical shift and the bond length (Figure 7) indicates that these large changes in the chemical shift primarily correspond to the stretching vibrations associated with the X−H bonds. The proton will experience a smaller shift when the X−H bond is contracted and a larger shift when it is extended. However, the time that the proton spends at the extremes of the bond is relatively short, which is reflected in the accompanying histograms in the rights panels (Figure 6). The histogram analyses of the calculated chemical shifts show a qualitatively normal distribution about the average values for the chemical shifts. This is consistent with the suggestion that the primary cause for the variation in the chemical shifts is the vibration of the bond; that is, the proton will spend the largest amount of time at, or around, the equilibrium position. The correlation coefficient is close to unity in each case (H46: 0.99; H63: 0.99; H59: 0.98). Clearly bending vibrations and interactions with neighboring nuclei will also influence the calculated chemical shift. However, the strong correlation between the bond length and the chemical shift indicates that the bond stretching vibration is the primary cause of the observed large fluctuations.

The large variations observed in this simulation differ from those reported previously in MM studies of the time evolution of NMR proton chemical shifts.[64,65] However, it is important to note that in these studies, only nonlocal contributions to the chemical shielding were considered. Moreover, the previously performed MM studies focused only on the proton chemical shifts, and in both cases, the H positions were either constrained or the H atoms were excluded from the simulation (using an extended atom approach) and subsequently added to the structure using the equilibrium values for bond lengths, angles, and so on. In either case, the variation in the relative H position is

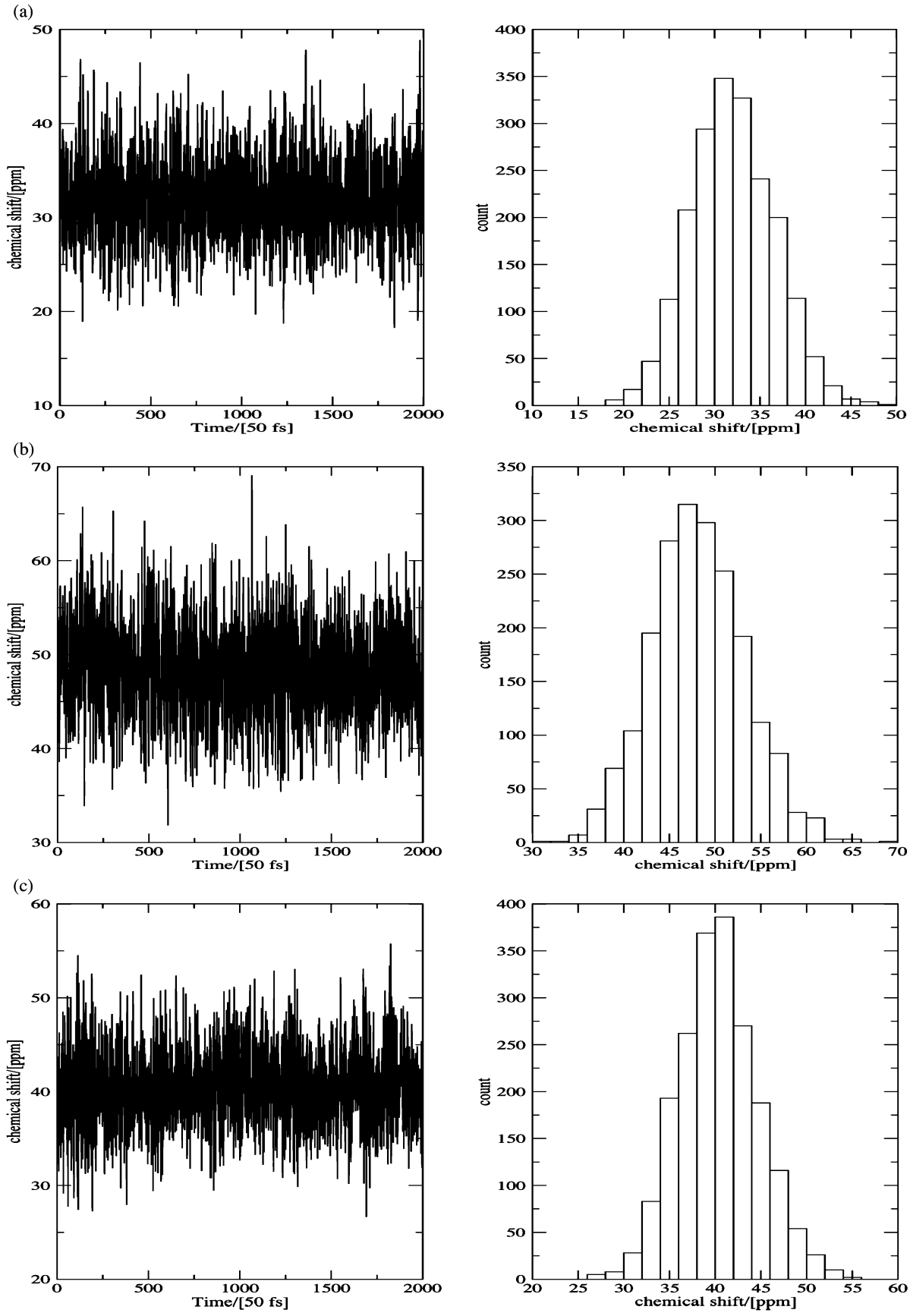

Figure 8. Time evolution of NMR chemical shifts for (a) C90: UE = 0.48 ppm; (b) C108: UE = 5.28 ppm; and (c) C58: UE = 13.89 ppm. Left: Variation in the ^{13}C NMR chemical shift as a function of time over the 100 ps simulation. Right: Distribution (bin width = 2.0 ppm) of the calculated chemical shifts for the 2000 snapshots taken at 50 fs intervals during the simulation.

excluded from the analysis, and it is only the changes in the environment to the proton, the nonlocal contributions to the chemical shielding, that affect the chemical shift. Therefore, in the current work, the smaller variations in the chemical shifts

that were observed in the previous studies are clearly swamped by the much larger variations in the chemical shielding that arise from the molecular vibrations.

There is no clear relationship between the standard deviation of the chemical shifts values about the average value (δ_{TAV}) and the resulting UE for the average value of the chemical shift, relative to the experimental reference value (δ_{ref}). The H46 atom ($\delta_{TAV} = 7.48$ ppm, $\delta_{ref} = 7.488$ ppm) has a UE of only 0.01 ppm; however, the standard deviation of the chemical shift values during the simulation ($\sigma_{H46} = 1.29$ ppm) is comparable to those atoms with larger UEs. H63 ($\delta_{TAV} = 2.30$ ppm, $\delta_{ref} = 0.855$ ppm) has a UE of 1.44 ppm, with only a marginally higher variation of the chemical shift during the simulation ($\sigma_{H63} = 1.46$). Finally, the proton with the largest UE (2.55 ppm), relative to the experimental value, is H59 ($\delta_{TAV} = 4.03$ ppm, $\delta_{ref} = 1.485$ ppm); however, the variation in the chemical shift for this atom is slightly smaller ($\sigma_{H59} = 1.44$) than that observed for H63, which has a smaller UE. Within the set of proton chemical shifts, there is also no clear relationship between the variation in the chemical shieldings over time and the magnitude of the time-averaged chemical shift. On the contrary, the standard deviation in the chemical shift is relatively consistent ($\sigma_{AV} = 1.50$ ppm, $\sigma_{\sigma} = 0.12$ ppm) across the range of ^{1}H chemical shifts, which is consistent with the dependence of the variation on the molecular vibrations that will remain relatively constant for the X—H bonds.

The variation of the ^{13}C NMR chemical shifts during the MD simulation follows a pattern similar to that of the ^{1}H NMR chemical shifts. The magnitude of the standard deviation for the ^{13}C NMR chemical shifts is larger than that observed for the ^{1}H NMR chemical shifts; however, as in the ^{1}H NMR shifts, the standard deviation is consistent within the set of ^{13}C NMR chemical shifts ($\sigma_{AV} = 4.8$ ppm, $\sigma_{\sigma} = 0.4$ ppm). The variation in the chemical shift again appears to depend on the local molecular vibrations; however, because the carbon atom can accommodate up to four bonds, the correlation with a single bond length is no longer informative. As observed for the ^{1}H NMR chemical shifts, there is no clear relationship between the standard deviation of the chemical shift values about the average value (δ_{TAV}) and the resulting UE for the average value of the chemical shift. For example, the C90 atom ($\delta_{TAV} = 32.0$ ppm, $\delta_{ref} = 31.5$ ppm) has a UE of 0.5 ppm, whereas the standard deviation of the chemical shift values during the simulation ($\sigma_{C90} = 4.6$ ppm) is comparable to C58 ($\delta_{TAV} = 40.4$ ppm, $\delta_{ref} = 26.5$ ppm), which has a standard deviation of ($\sigma_{C58} = 4.3$ ppm). C108 ($\delta_{TAV} = 48.2$ ppm, $\delta_{ref} = 42.9$ ppm) has a slightly larger standard deviation ($\sigma_{C108} = 5.1$ ppm), although it is still within one standard deviation of the mean.

4. Conclusions

The current work highlights the variability of the calculated chemical shift over the short time scale of molecular vibrations that are experienced during a molecular dynamics simulation. In the case of ^{1}H NMR chemical shifts, the calculated values were found to fluctuate by up to 10 ppm between snapshots, whereas the ^{13}C NMR chemical shift fluctuations were as large as 40 ppm. These fluctuations can be attributed to the molecular vibrations that occur on these time scales. Despite the magnitude of these vibrations, the time-averaged chemical shifts are able to reproduce the experimental values with reasonable accuracy given the lack of conformational sampling, as long as an appropriately large ensemble of the structures is selected to obtain an equilibrium value for the molecular vibrations. Clearly, if individual snapshots of the simulation are viewed in isolation, then the calculated chemical shifts may provide wildly different results than those obtained experimentally.

The systematic overestimation of the ^{1}H and ^{13}C NMR chemical shifts that remain can be attributed to either methodological error that arises from the necessary simplifications in the semiempirical framework or, alternatively, from an insufficient sampling period. The time-averaged chemical shifts calculated in this work concentrate on the effect of molecular vibrations on the measured chemical shifts with only minor conformational changes occurring during the simulation. However, because experimental chemical shifts are measured on the millisecond time scale, there will be a number of conformers that will also contribute to the experimental value. However, the time scales required to investigate these larger changes were not the focus of the current work.

The time-averaged chemical shifts improve upon the average chemical shifts that are obtained from the optimized structures of low-energy conformers. Whereas the MUE of the time-averaged chemical shifts is comparable to that obtained for the average of the optimized conformers, the variability in the errors is decreased as a result of the simulation. The decreased variability is attributed to the removal of unrealistic features in the gas-phase optimized structures (strong intramolecular H bonds) during the simulation. Therefore, gas-phase optimized structures should be used only in conjunction with appropriate constraints that more closely model those imposed by the environment.

The OM3 and OM3-D QM methods, in combination with the CHARMM MM method, provide a reliable description of the dynamics of the heptatpeptide in solution over the 100 ps QM/MM simulation. The semiempirical NMR method is also able to provide accurate results for the nonequilibrium structures that are encountered during the simulation, such that the resulting time-averaged chemical shifts are comparable to the experimental values.

Acknowledgment. The author acknowledges the Royal Society of Edinburgh for support through a Scottish Executive Personal Research Fellowship, the EPSRC for funding (EP/F031769), and the Glasgow Centre for Physical Organic Chemistry.

Supporting Information Available: Details of the calculated average chemical shifts for the optimized structures and the time-averaged chemical shifts from the MD simulations are provided. The final optimized structures of the 20 conformers are available in PDB format. This material is available free of charge via the Internet at http://pubs.acs.org.

References and Notes

(1) Wuthrich, K. *NMR of Proteins and Nucleic Acids*; Wiley: New York, 1986.
(2) Spera, S.; Bax, A. *J. Am. Chem. Soc.* **1991**, *113*, 5490.
(3) Wishart, D. S.; Sykes, B. D.; Richards, F. M. *Biochemistry* **1992**, *31*, 1647.
(4) Dedios, A. C.; Pearson, J. G.; Oldfield, E. *Science* **1993**, *260*, 1491.
(5) Wishart, D. S.; Bigam, C. G.; Yao, J.; Abildgaard, F.; Dyson, H. J.; Oldfield, E.; Markley, J. L.; Sykes, B. D. *J. Biomol. NMR* **1995**, *6*, 135.
(6) Lepre, C. A.; Moore, J. M.; Peng, J. W. *Chem. Rev.* **2004**, *104*, 3641.
(7) Koch, W.; Holthausen, M. C. *A Chemist's Guide to Density Functional Theory*, 2nd ed.; Wiley-VCH: Weinheim, Germany, 2002.
(8) Neal, S.; Nip, A. M.; Zhang, H. Y.; Wishart, D. S. *J. Biomol. NMR* **2003**, *26*, 215.
(9) Osapay, K.; Case, D. A. *J. Am. Chem. Soc.* **1991**, *113*, 9436.
(10) Wu, W. X.; You, X. Z.; Dai, A. B. *Sci. Sin., Ser. B (Engl. Ed.)* **1988**, *31*, 1048.
(11) Patchkovskii, S.; Thiel, W. *J. Comput. Chem.* **1999**, *20*, 1220.

(12) Bing, W.; Raha, K.; Merz, K. M. *J. Am. Chem. Soc.* **2004**, *126*, 11430.
(13) Chen, Z. F.; Thiel, W. *Chem. Phys. Lett.* **2003**, *367*, 15.
(14) De Proft, F.; Geerlings, P. *Chem. Rev.* **2001**, *101*, 1451.
(15) Lomas, J. S.; Maurel, F. *J. Phys. Org. Chem.* **2008**, *21*, 464.
(16) Patchkovskii, S.; Thiel, W. *J. Mol. Model.* **2000**, *6*, 67.
(17) Smith, S. K.; Cobleigh, J.; Svetnik, V. *J. Chem. Inf. Comput. Sci.* **2001**, *41*, 1463.
(18) Wang, B.; Brothers, E. N.; van der Vaart, A.; Merz, K. M. *J. Chem. Phys.* **2004**, *120*, 11392.
(19) Wang, B.; Merz, K. M. *J. Chem. Theory Comput.* **2006**, *2*, 209.
(20) Wang, B.; Miskolzie, M.; Kotovych, G.; Pulay, P. *J. Biomol. Struct. Dyn.* **2002**, *20*, 71.
(21) Williams, D. E.; Peters, M. B.; Wang, B.; Merz, K. M. *J. Phys. Chem. A* **2008**, *112*, 8829.
(22) Daura, X.; Antes, I.; van Gunsteren, W. F.; Thiel, W.; Mark, A. E. *Proteins: Struct., Funct., Genet.* **1999**, *36*, 542.
(23) Binetruy-Tournaire, R.; Demangel, C.; Malavaud, B.; Vassy, R.; Rouyre, S.; Kraemer, M.; Plouet, J.; Derbin, C.; Perret, G.; Mazie, J. C. *EMBO J.* **2000**, *19*, 1525.
(24) Starzec, A.; Ladam, P.; Vassy, R.; Badache, S.; Bouchemal, N.; Navaza, A.; Du Penhoat, C. H.; Perret, G. Y. *Peptides* **2007**, *28*, 2397.
(25) Overlapping is defined by the distance between the TIP3P oxygen atom and any non-TIP3P heavy atom: R(O-X). If R(O-X) <2.8 Å, then the TIP3P water is deleted.
(26) Brooks, C. L.; Karplus, M. *J. Chem. Phys.* **1983**, *79*, 6312.
(27) *CHARMM*, version c31b1; Department of Chemistry and Chemical Biology, Harvard University: Cambridge, MA, 2004.
(28) Brooks, B. R.; Bruccoleri, R. E.; Olafson, B. D.; States, D. J.; Swaminathan, S.; Karplus, M. *J. Comput. Chem.* **1983**, *4*, 187.
(29) MacKerell, A. D.; Brooks, B. R.; Brooks, C. L., III; Nilsson, L.; Roux, B.; Won, Y.; Karplus, M. In *Encyclopedia of Computational Chemistry*; Schleyer, P. v. R., Ed.; Wiley: Chichester, U.K., 1998; Vol. 1, p 271.
(30) MacKerell, A. D.; Bashford, D.; Bellott, M.; Dunbrack, R. L.; Evanseck, J. D.; Field, M. J.; Fischer, S.; Gao, J.; Guo, H.; Ha, S.; Joseph-McCarthy, D.; Kuchnir, L.; Kuczera, K.; Lau, F. T. K.; Mattos, C.; Michnick, S.; Ngo, T.; Nguyen, D. T.; Prodhom, B.; Reiher, W. E.; Roux, B.; Schlenkrich, M.; Smith, J. C.; Stote, R.; Straub, J.; Watanabe, M.; Wiorkiewicz-Kuczera, J.; Yin, D.; Karplus, M. *J. Phys. Chem. B* **1998**, *102*, 3586.
(31) Scholten, M. Ph.D. Thesis, Universität Düsseldorf: Düsseldorf, Germany, 2003.
(32) Tuttle, T.; Thiel, W. *Phys. Chem. Chem. Phys.* **2008**, *10*, 2159.
(33) *ChemShell*, version 3.0a3; CCLRC Daresbury Laboratory: Cheshire, U.K., 2004.
(34) Sherwood, P.; de Vries, A. H.; Guest, M. F.; Schreckenbach, G.; Catlow, C. R. A.; French, S. A.; Sokol, A. A.; Bromley, S. T.; Thiel, W.; Turner, A. J.; Billeter, S.; Terstegen, F.; Thiel, S.; Kendrick, J.; Rogers, S. C.; Casci, J.; Watson, M.; King, F.; Karlsen, E.; Sjøvoll, M.; Fahmi, A.; Schäfer, A.; Lennartz, C. *THEOCHEM* **2003**, *632*, 1.
(35) Thiel, W. *MNDO04*, version 6.1; Max-Planck-Institut für Kohlenforschung: Mülheim an der Ruhr, Germany, 2004.
(36) Berendsen, H. J. C.; Postma, J. P. M.; van Gunsteren, W. F.; Dinola, A.; Haak, J. R. *J. Chem. Phys.* **1984**, *81*, 3684.
(37) Hoover, W. G. *Phys. Rev. A* **1985**, *31*, 1695.
(38) Nose, S. *J. Chem. Phys.* **1984**, *81*, 511.
(39) Nose, S. *Mol. Phys.* **1984**, *52*, 255.
(40) Ryckaert, J. P.; Ciccotti, G.; Berendsen, H. J. C. *J. Comput. Phys.* **1977**, *23*, 327.
(41) Billeter, S. R.; Turner, A. J.; Thiel, W. *Phys. Chem. Chem. Phys.* **2000**, *2*, 2177.
(42) Dewar, M. J. S.; Thiel, W. *J. Am. Chem. Soc.* **1977**, *99*, 4899.
(43) Ditchfield, R. *J. Chem. Phys.* **1972**, *56*, 5688.
(44) Wolinski, K.; Hinton, J. F.; Pulay, P. *J. Am. Chem. Soc.* **1990**, *112*, 8251.
(45) *TURBOMOLE*, V. 5.10.1; COSMO logic G.m.b.H & Co. KG: Leverkusen, Germany, 2008.
(46) Ahlrichs, R.; Bär, M.; Häser, M.; Horn, H.; Kölmel, C. *Chem. Phys. Lett.* **1989**, *162*, 165.
(47) Eichkorn, K.; Treutler, O.; Ohm, H.; Häser, M.; Ahlrichs, R. *Chem. Phys. Lett.* **1995**, *242*, 652.
(48) Treutler, O.; Ahlrichs, R. *J. Chem. Phys.* **1995**, *102*, 346.
(49) Eichkorn, K.; Treutler, O.; Ohm, H.; Häser, M.; Ahlrichs, R. *Chem. Phys. Lett.* **1995**, *240*, 283.
(50) Becke, A. D. *Phys. Rev. A* **1988**, *38*, 3098.
(51) Perdew, J. P. *Phys. Rev. B* **1986**, *33*, 8822.
(52) Vosko, S. H.; Wilk, L.; Nusair, M. *Can. J. Phys.* **1980**, *58*, 1200.
(53) Weigend, F.; Ahlrichs, R. *Phys. Chem. Chem. Phys.* **2005**, *7*, 3297.
(54) Grimme, S. *J. Comput. Chem.* **2006**, *27*, 1787.
(55) Frisch, M. J.; Trucks, G. W.; Schlegel, H. B.; Scuseria, G. E.; Robb, M. A.; Cheeseman, J. R.; Montgomery, J. A., Jr.; Vreven, T.; Kudin, K. N.; Burant, J. C.; Millam, J. M.; Iyengar, S. S.; Tomasi, J.; Barone, V.; Mennucci, B.; Cossi, M.; Scalmani, G.; Rega, N.; Petersson, G. A.; Nakatsuji, H.; Hada, M.; Ehara, M.; Toyota, K.; Fukuda, R.; Hasegawa, J.; Ishida, M.; Nakajima, T.; Honda, Y.; Kitao, O.; Nakai, H.; Klene, M.; Li, X.; Knox, J. E.; Hratchian, H. P.; Cross, J. B.; Bakken, V.; Adamo, C.; Jaramillo, J.; Gomperts, R.; Stratmann, R. E.; Yazyev, O.; Austin, A. J.; Cammi, R.; Pomelli, C.; Ochterski, J. W.; Ayala, P. Y.; Morokuma, K.; Voth, G. A.; Salvador, P.; Dannenberg, J. J.; Zakrzewski, V. G.; Dapprich, S.; Daniels, A. D.; Strain, M. C.; Farkas, O.; Malick, D. K.; Rabuck, A. D.; Raghavachari, K.; Foresman, J. B.; Ortiz, J. V.; Cui, Q.; Baboul, A. G.; Clifford, S.; Cioslowski, J.; Stefanov, B. B.; Liu, G.; Liashenko, A.; Piskorz, P.; Komaromi, I.; Martin, R. L.; Fox, D. J.; Keith, T.; Al-Laham, M. A.; Peng, C. Y.; Nanayakkara, A.; Challacombe, M.; Gill, P. M. W.; Johnson, B.; Chen, W.; Wong, M. W.; Gonzalez, C.; Pople, J. A. *Gaussian 03*, V. E.01; Gaussian, Inc.: Wallingford, CT, 2004.
(56) Becke, A. D. *J. Chem. Phys.* **1993**, *98*, 5648.
(57) Hertwig, R. H.; Koch, W. *Chem. Phys. Lett.* **1997**, *268*, 345.
(58) Lee, C. T.; Yang, W. T.; Parr, R. G. *Phys. Rev. B* **1988**, *37*, 785.
(59) Stephens, P. J.; Devlin, F. J.; Chabalowski, C. F.; Frisch, M. J. *J. Phys. Chem.* **1994**, *98*, 11623.
(60) Hariharan, P. C.; Pople, J. A. *Theor. Chim. Acta* **1973**, *28*, 213.
(61) Krishnan, R.; Binkley, J. S.; Seeger, R.; Pople, J. A. *J. Chem. Phys.* **1980**, *72*, 650.
(62) Rablen, P. R.; Pearlman, S. A.; Finkbiner, J. *J. Phys. Chem. A* **1999**, *103*, 7357.
(63) Otte, N.; Scholten, M.; Thiel, W. *J. Phys. Chem. A* **2007**, *111*, 5751.
(64) Hoch, J. C.; Dobson, C. M.; Karplus, M. *Biochemistry* **1982**, *21*, 1118.
(65) Nowakowski, J.; Miller, J. L.; Kollman, P. A.; Tinoco, I. *J. Am. Chem. Soc.* **1996**, *118*, 12812.

JP902875D